Experimental Evidence for the Elusive Ketohydroperoxide Pathway and the Formation of Glyoxal in Ethylene Ozonolysis

Caroline Smith Lewin, Olivier Herbinet, Gustavo A Garcia, Philippe Arnoux, Luc-Sy Tran, Guillaume Vanhove, Laurent Nahon, Frederique Battin-Leclerc, Jérémy Bourgalais

COMMUNICATION

Experimental Evidence for the Elusive Ketohydroperoxide Pathway and the Formation of Glyoxal in Ethylene Ozonolysis

Received 00th January 20xx,
Accepted 00th January 20xx

DOI: 10.1039/x0xx00000x

Caroline Smith Lewin,[a] Olivier Herbinet,[a] Gustavo A. Garcia,[b] Philippe Arnoux,[a] Luc-Sy Tran,[c] Guillaume Vanhove,[c] Laurent Nahon,[b] Frédérique Battin-Leclerc,[a] and Jérémy Bourgalais*[a]

Despite decades of research on alkene ozonolysis, the kinetic network of the archetypal case of ethylene (CH_2=CH_2) with ozone (O_3) still lacks consensus. In this work, experimental evidence of a diradical pathway is provided through the detection of the 2-hydroperoxyacetaldehyde ketohydroperoxide and its decomposition product, glyoxal.

Alkene ozonolysis is the source of a significant fraction of tropospheric submicron secondary organic aerosols (SOA). A single bimolecular reaction between a volatile organic compound (VOC) and ozone (O_3) triggers rapid gas-phase autoxidation processes leading to low-volatility highly oxygenated molecules (HOM) which are prone to condense and contribute to the formation of new particles.[1–3] However, structural elucidation of HOM is far from being achieved, even in extensively studied archetypal systems. Current molecular mechanisms are unable to explain the high HOM yield measured from alkene ozonolysis.[4,5] The formation mechanisms of SOA thus remain largely unknown and their impact on climate modulation is still an open key question.[6]

Alkene ozonolysis therefore remains a very active research field, even for the smallest system: C_2H_4 + O_3 as shown by the recent vivid scientific production,[7–14] while the first research traces back to the middle of the 19th century.[15] Ethylene is one of the organics that accompanied α-pinene emissions in forestland areas.[16] The first steps of ethylene ozonolysis have been known for a long time (see Figure 1): an exothermic cycloaddition of O_3 forming a cyclic primary ozonide (POZ), which then undergoes a concerted cycloreversion from homolytic O-O and C-C cleavage bond leading to a reactive CH_2OO Criegee intermediate (CI) and formaldehyde as a co-product (see Osborn & Taatjes and Taatjes for recent reviews on CI).[17,18] However, recent studies predict that a dissociation can occur in two steps forming a diradical intermediate of which a significant fraction (> 10%) yield, via an internal H-atom migration, a 2-hydroperoxyacetaldehyde (HPA) which is a ketohydroperoxide.[7,10]

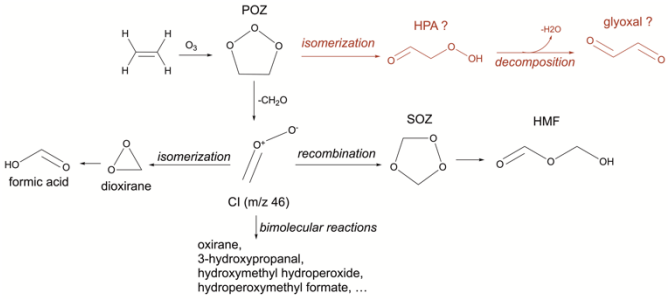

Figure 1. Simplified scheme of the main known reaction pathways and intermediates in ethylene ozonolysis based on literature. In red, the elusive ketohydroperoxide pathway which is the scope of this work.

Experimentally, the direct observation of HPA in ethylene ozonolysis has only been reported by Rousso et al.[9] using synchrotron vacuum ultraviolet photoionization mass spectrometry (SVUV-PIMS). The detection of HPA was based on the correlation between the ionization threshold in the recorded total ion yield (TIY) curve of m/z 76 and the calculated adiabatic ionization energy (AIE) of HPA. Following this detection Porterfield et al.[11] were, however, unable to detect HPA using microwave spectroscopy despite close experimental conditions. They were able though, to detect the highly reactive hydroperoxymethyl formate ($HCOCH_2OOH$, HPMF). To explain the non-observation of HPA in the work of Porterfield et al.[11], Genossar et al.[13] predicted a new decomposition pathway of HPA by the successive removal of an OH radical and a H-atom that would lead to the simplest dione, glyoxal (HCOCHO). Ozonolysis initiates a sequence of exothermic reactions leading to the formation of vibrationally excited reactive intermediates with weak bonds. The excess of internal energy could lead to fast decomposition of these intermediates that can prevent their experimental detection under insufficient collisional stabilization conditions. Rousso et al.[12] recorded a signal at m/z 58 though without discussing its origin.

Beyond the fundamental interest of studying the competition between dissociation, isomerization and stabilization, the

[a] Université de Lorraine, CNRS, LRGP, F-54000 Nancy, France.
[b] Synchrotron SOLEIL, L'Orme des merisiers, Saint-Aubin-BP 48, 91192 Gif-sur-Yvette Cedex, France.
[c] Université Lille, CNRS, UMR 8522 - PC2A - Physicochimie des Processus de Combustion et de l'Atmosphère, F-59000 Lille, France.

Electronic Supplementary Information (ESI) available: [Scheme of the experimental setup and additional SPES and theoretical calculations]. See DOI: 10.1039/x0xx00000x

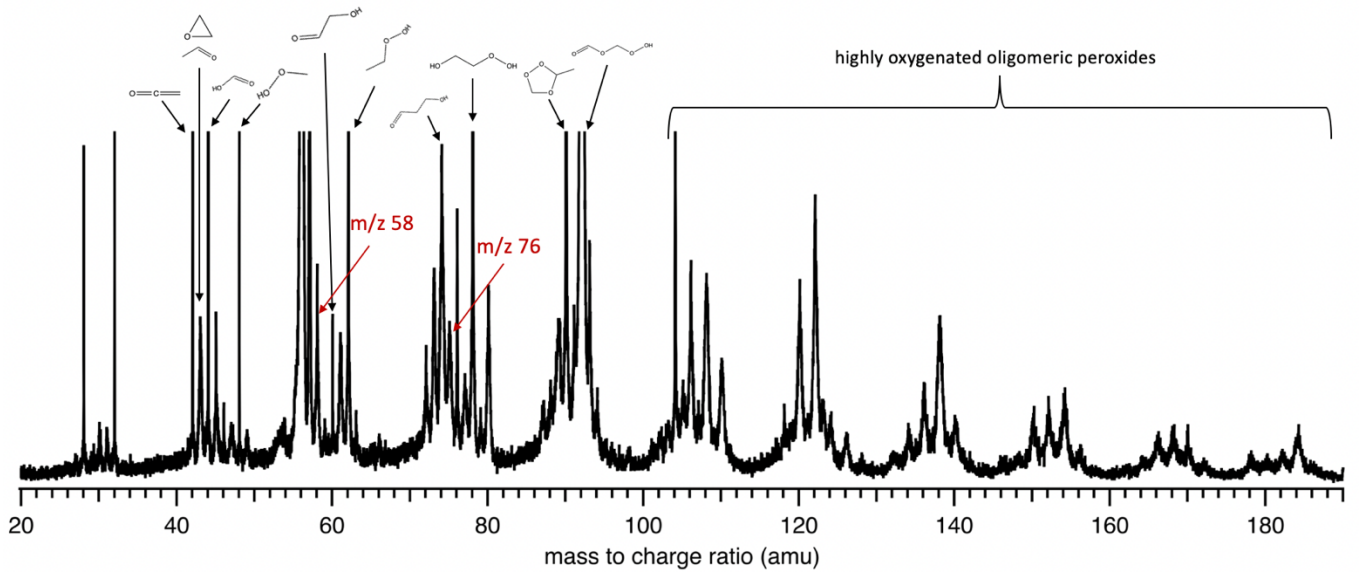

Figure 2. Typical mass spectrum recorded by synchrotron photoionization of a $He/O_2/O_3/C_2H_4$ gas mixture integrated over the 9.0 – 10.4 eV photon energy range at room temperature. The structure of some already known intermediates based on literature is also displayed.

diradical pathway is of special interest for atmospheric chemistry. The decomposition of ketohydroperoxides in autoxidation chemical systems can produce a pool of OH radicals[19] while glyoxal is the most abundant atmospheric dicarbonyl species and known as a SOA precursor due to its hydrophilic functionality.[20,21]

Here, we demonstrate experimentally the unambiguous formation of both HPA and glyoxal. A gas mixture made of C_2H_4, He, O_2, and O_3 was adiabatically expanded through a 200 micrometer sized nozzle into the SAPHIRS permanent photoionization end-station[22] at the DESIRS vacuum ultraviolet beamline of synchrotron SOLEIL.[23] The nozzle was mounted at the tip of a movable hollow rod connecting the gas line to the SAPHIRS expansion chamber. C_2H_4 and O_3 were mixed before entering the rod (see Figure S1). The residence time of the gas inside the rod was measured to be ~1 minute based on the response of an O_3-analyser located at the main outlet. The experiments were done at room temperature. The O_3 mole fraction was monitored before and after the experiments and measured to be ~3,000 ppm. During the experiments, the O_3 mixing ratio went down to 60 ppm corresponding to a conversion of about 98% of O_3 in the process. The flows, given in $mL.min^{-1}$, were 1,180 (He, 84%), 176 (O_2, 13%), and 35 (C_2H_4, 2%). Note that a similar gas mixture was used in a jet-stirred reactor (JSR) at LRGP upstream of the synchrotron measurement campaign. The O_3 molar fraction at the JSR outlet was measured experimentally by an O_3 analyzer and simulated with a gas-phase chemical kinetic model[24]. A good agreement was found between the predictions of the kinetic model and the experimental measurements showing that wall reactions are negligible in this experimental configuration. The resulting vapor was doubly skimmed before reaching the ionization chamber where it crossed the synchrotron radiation at the center of the DELICIOUS III double imaging photoelectron/photoion coincidence (i^2PEPICO) spectrometer.[25] Electrons and ions are accelerated perpendicularly by a constant electric field, towards a velocity map imager and a modified Wiley-McLaren time of flight 3D-momentum imaging analyzer respectively.[26,27] The coincidence scheme yields mass-selected photoelectron images which are then Abel inverted[28] to obtain mass-selected photoelectron spectra (PES). The coincidence signal can then be plotted as a function of electron and photon energy, from which the slow photoelectron spectra (SPES) are obtained by integration of the 2D matrix along a low kinetic energy band.[29,30] SPES provides information on the electronic structures of the isomers present which can then be identified by comparison with literature reference spectra of individual species. When reference spectra are not yet reported in the literature, analyses are supported by high-level theoretical quantum calculations, which provide the simulated PES of the molecular species of interest (see SI for more explanations regarding the theoretical method).

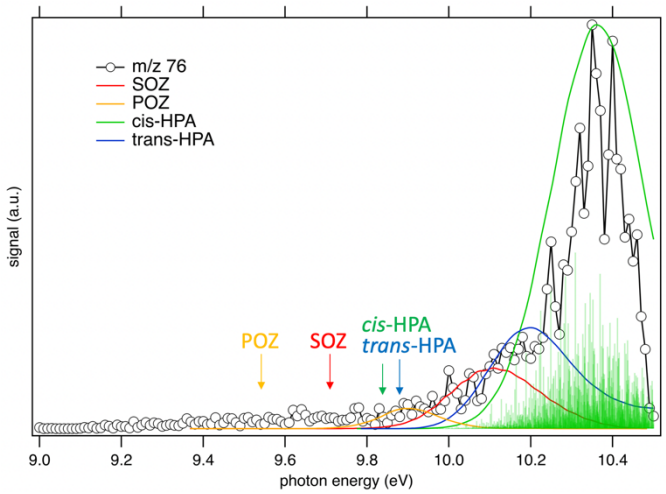

Figure 3. SPES of m/z 76 (open dots) compared to the simulated spectra of *cis*-HPA (green line), trans-HPA, SOZ, and POZ (orange line). Arrows indicate the calculated AIE of the $C_2H_4O_3$ isomers at the CCSD(T)/CBS level. The computed stick spectrum of *cis*-HPA is also displayed (green light sticks) and together with its respective simulated spectrum have been shifted by 80 meV from the calculated AIE. The stick spectrum of the other $C_2H_4O_3$ isomers is provided in Figure S2.

Figure 2 shows a typical mass spectrum recorded by synchrotron photoionization of a $He/O_2/O_3/C_2H_4$ gas mixture integrated over the 9.0 – 10.4 eV photon energy range at room temperature. The most intense peaks had to be cut off to make peaks with lower signal intensity better visible. The mass spectrum reported in Figure 2 is comparable to ones obtained in Rousso et al.[12]. The m/z 92 assigned to HPMF in the literature is the second highest peak in Figure 2 and is consistent with the role of atmospheric aerosol precursors that is assigned to hydroperoxide esters.[11] The structure of other already known intermediates based on literature are also displayed, but one can note that many peaks have yet to be assigned, especially those above m/z 100 assigned to oligomeric hydroperoxides. Due to their importance in the formation of SOA in the atmosphere,[31–33] the structure of such large poly-oxygenated molecules will be evaluated in a future study.

Here, the main focus is on the species related to the diradical pathway whose masses are highlighted by a red arrows in Figure 2. Figure 3 shows the SPES of m/z 76 compared to simulated spectra of $C_2H_4O_3$ isomers (POZ, SOZ, *cis*-HPA, and *trans*-HPA). Hydroxymethyl formate (HMF) has been considered in this work but ruled out based on its calculated AIE above 10.5 eV (see Table S1). Note that the AIE calculations were carried out at the CCSD(T)/CBS and CBS-QB3 levels and that they are in good agreement for all the species except for the ketohydroperoxide. CCSD(T)/CBS energies were extrapolated from energies calculated with different basis set size (see SI). Relatively significant differences were found in the AIE by increasing the basis set size highlighting that the electronic wave function is not well defined probably due to the flexibility of the ketohydroperoxide structure.[34] The analysis based on the respective AIEs and simulated spectra shows that *cis*-HPA is the main contributor to the signature of the SPES of m/z 76 below 10.5 eV. Potential minor contribution from *trans*-HPA, SOZ, and POZ cannot be ruled out though. Especially, according to the small energy difference with the *trans*-conformation (1 kcal mol^{-1}) and the exothermicity of the reaction (~100 kcal mol^{-1}),[13] both *cis/trans* configurations could be present in the current experimental conditions. The present analysis of the SPES of m/z 76 with detection of the *cis*-conformation of HPA supports the findings of Rousso et al.[9]. Additionally, the SPES of m/z 122 fits with a simulated spectrum of 3-(hydroperoxymethyl)-1,2,4-trioxolane that can be formed assuming a cycloaddition of the CI to the aldehyde function of HPA (see Figure S3). Note that based on the analysis other $C_3H_6O_5$ isomers could also contribute. This result supports the sequential insertion reactions proposed by Rousso et al.[12] to explain the large distribution of products in ethylene ozonolysis. This results also demonstrates that addition on the carbonyl function can be competitive with the OH-insertion suggested by Rousso et al.[12] and that insertion reactions are fast enough to compete with the HPA dissociation.

Genossar et al.[13] also suggested that decomposition of HPA would mainly lead to the formation of glyoxal considering the removal of one H-atom from the formylmethoxy radical after the O-O bond cleavage. Note that this decomposition mechanism is different from the conventional OOH-loss

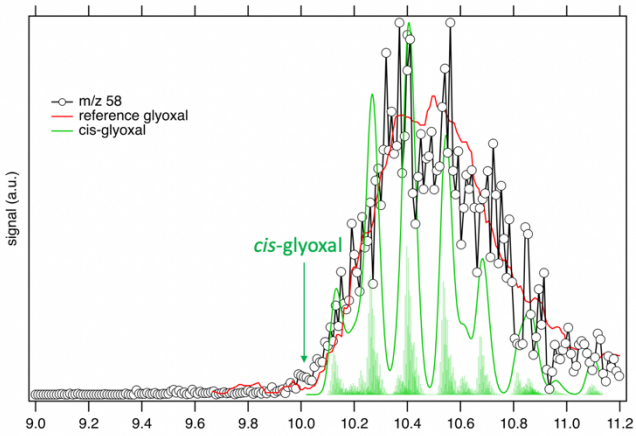

Figure 4. SPES of m/z 58 (open dots) compared to a simulated spectrum of *cis*-glyoxal (green line) and a reference threshold photoelectron spectrum of glyoxal (red line). The arrow indicates the calculated AIE of *cis*-glyoxal using the CCSD(T)/CBS limit method. The computed stick spectrum of *cis*-HPA is also displayed (green light sticks) and together with its respective simulated spectrum have been shifted by 80 meV from the calculated AIE.

assumed for ketohydroperoxide in autoxidation chemistry.[19] An ion signal is detected at m/z 58 in this work (see Figure 2) and the respective recorded SPES is shown in Figure 4. The SPES fits well with a reference threshold photoelectron spectrum of glyoxal from Baeza-Romero et al.[35]. The observed ionization threshold fits also well with the calculated AIE of *cis*-glyoxal (see Table S1) and the simulated spectrum of *cis*-glyoxal displays sharp structures similar to the ones observed in the recorded experimental spectrum. The calculated AIE of *trans*-glyoxal found above the observed ionization threshold and its respective simulated spectrum (see Figure S4 for the computed stick spectrum) do not allow to address the formation of *trans*-glyoxal in this work. This result also confirms that the formation of *cis*-glyoxal is possible under thermalized conditions, as assumed by Genossar et al.[13]. Additionally, the SPES of m/z 104 shown in Figure S5 fits well with simulated spectra of isomers that would be formed via CH-insertion of the CI to glyoxal or cycloaddition. Finally, this result supports the molecular growth mechanism based on successive CI reactions with intermediates proposed by Rousso et al.[12].

In conclusion, this work unambiguously confirms that a substantial fraction of the POZ isomerizes into the HPA ketohydroperoxide which is consistent with the findings estimated by Pfeifler et al.[10]. This work also confirms that a significant proportion of HPA decomposes to glyoxal. The decomposition of HPA must occur within the ~1 minute residence time but since HPA is detected the reaction is not that fast neither. The detection of *cis*-glyoxal makes a validation by microwave spectroscopy possible because, unlike *trans*-glyoxal, it has a non-vanishing dipole moment. The oxidation of C_2H_4 is known as a main glyoxal contributor in the troposphere but via the reaction between OH and glycolaldehyde.[36] However, there is a general model underestimation of the glyoxal measured *in situ* and especially during the night where OH concentration depletes.[37] It would thus be interesting to implement this direct source of glyoxal from C_2H_4 ozonolysis and see if it could overcome this disagreement.

Conflicts of interest

There are no conflicts to declare.

References

1 M. Ehn, J. A. Thornton, E. Kleist, et al., *Nature*, 2014, **506**, 476–479.

2 S. Schobesberger, H. Junninen, F. Bianchi, et al., *Proc. Natl. Acad. Sci. U.S.A.*, 2013, **110**, 17223–17228.

3 F. Riccobono, S. Schobesberger, C. E. Scott, et al., *Science*, 2014, **344**, 717–721.

4 M. Ehn, T. Berndt, J. Wildt and T. Mentel, *International Journal of Chemical Kinetics*, 2017, **49**, 821–831.

5 S. Iyer, M. P. Rissanen, R. Valiev, S. Barua, J. E. Krechmer, J. Thornton, M. Ehn and T. Kurtén, *Nat Commun*, 2021, **12**, 878.

6 P. Stier, N. a. J. Schutgens, N. Bellouin, et al., *Atmospheric Chemistry and Physics*, 2013, **13**, 3245–3270.

7 T. L. Nguyen, H. Lee, D. A. Matthews, M. C. McCarthy and J. F. Stanton, *J. Phys. Chem. A*, 2015, **119**, 5524–5533.

8 C. C. Womack, M.-A. Martin-Drumel, G. G. Brown, R. W. Field and M. C. McCarthy, *Sci. Adv.*, 2015, **1**, e1400105.

9 A. C. Rousso, N. Hansen, A. W. Jasper and Y. Ju, *J. Phys. Chem. A*, 2018, **122**, 8674–8685.

10 M. Pfeifle, Y.-T. Ma, A. W. Jasper, L. B. Harding, W. L. Hase and S. J. Klippenstein, *J. Chem. Phys.*, 2018, **148**, 174306.

11 J. P. Porterfield, K. L. K. Lee, V. Dell'Isola, P. B. Carroll and M. C. McCarthy, *Phys. Chem. Chem. Phys.*, 2019, **21**, 18065–18070.

12 A. C. Rousso, N. Hansen, A. W. Jasper and Y. Ju, *Physical Chemistry Chemical Physics*, 2019, **21**, 7341–7357.

13 N. Genossar, J. P. Porterfield and J. H. Baraban, *Phys. Chem. Chem. Phys.*, 2020, **22**, 16949–16955.

14 M. Chen, S. Tong, Z. Wang, W. Li, Y. Xu, S. Wang and M. Ge, *Journal of Environmental Sciences*, 2021, **105**, 128–137.

15 M. B. Rubin, *Bull. Hist. Chem.*, 2001, **26**, 17.

16 P. R. Zimmerman, J. P. Greenberg and C. E. Westberg, *Journal of Geophysical Research: Atmospheres*, 1988, **93**, 1407–1416.

17 C. A. Taatjes, *Annual Review of Physical Chemistry*, 2017, **68**, 183–207.

18 D. L. Osborn and C. A. Taatjes, *International Reviews in Physical Chemistry*, 2015, **34**, 309–360.

19 Z. Wang, O. Herbinet, N. Hansen and F. Battin-Leclerc, *Progress in Energy and Combustion Science*, 2019, **73**, 132–181.

20 J. Hu, Z. Chen, X. Qin and P. Dong, *Atmospheric Chemistry and Physics*, 2022, **22**, 6971–6987.

21 Z. Ling, Q. Xie, M. Shao, Z. Wang, T. Wang, H. Guo and X. Wang, *Atmospheric Chemistry and Physics*, 2020, **20**, 11451–11467.

22 X. Tang, G. A. Garcia, J.-F. Gil and L. Nahon, *Review of Scientific Instruments*, 2015, **86**, 123108.

23 L. Nahon, N. de Oliveira, G. A. Garcia, et al., *J Synchrotron Rad*, 2012, **19**, 508–520.

24 C. Smith Lewin, O. Herbinet, F. Battin-Leclerc and J. Bourgalais, *Chemical Physics Letters*, 2022, **806**, 139986.

25 G. A. Garcia, B. K. Cunha de Miranda, M. Tia, S. Daly and L. Nahon, *Review of Scientific Instruments*, 2013, **84**, 053112.

26 D. H. Parker and A. T. J. B. Eppink, *J. Chem. Phys.*, 1997, **107**, 2357–2362.

27 W. C. Wiley and I. H. McLaren, *Review of Scientific Instruments*, 1955, **26**, 1150–1157.

28 G. A. Garcia, L. Nahon and I. Powis, *Review of Scientific Instruments*, 2004, **75**, 4989–4996.

29 J. C. Poully, J. P. Schermann, N. Nieuwjaer, et al., *Physical Chemistry Chemical Physics*, 2010, **12**, 3566–3572.

30 M. Briant, L. Poisson, M. Hochlaf, P. de Pujo, M.-A. Gaveau and B. Soep, *Phys. Rev. Lett.*, 2012, **109**, 193401.

31 L. Vereecken, A. R. Rickard, M. J. Newland and W. J. Bloss, *Phys. Chem. Chem. Phys.*, 2015, **17**, 23847–23858.

32 S. V. Tadayon, E. S. Foreman and C. Murray, *J. Phys. Chem. A*, 2018, **122**, 258–268.

33 Y. Sakamoto, S. Inomata and J. Hirokawa, *J. Phys. Chem. A*, 2013, **117**, 12912–12921.

34 J. Bourgalais, Z. Jiang, J. Bloino, et al., *Phys. Chem. Chem. Phys.*, 2022, **24**, 10826.

35 M. T. Baeza-Romero, F. Gaie-Levrel, A. Mahjoub, V. López-Arza, G. A. Garcia and L. Nahon, *Eur. Phys. J. D*, 2016, **70**, 154.

36 N. I. Butkovskaya, N. Pouvesle, A. Kukui and G. Le Bras, *J. Phys. Chem. A*, 2006, **110**, 13492–13499.

37 H. Walker, D. Stone, T. Ingham, et al., *Atmospheric Chemistry and Physics*, 2022, **22**, 5535–5557.